Morphology Development of 10-μm Scale Polymer Particles Prepared by SPG Emulsification and Suspension Polymerization

SHINZO OMI, TATSUO SENBA, MASATOSHI NAGAI, GUANG-HUI MA

Graduate School of Bio-Applications and Systems Engineering, Tokyo University of Agriculture and Technology, Nakamachi, Koganei, Tokyo 184-8588, Japan

Received 19 February 2000; accepted 17 May 2000

ABSTRACT: Classical particle morphologies, core-shell, hemisphere, sandwich, and so on, were all reproducible by starting from ca. 10-μm uniform droplets composed of monomers, initiator, solvents, and polymer, and polymerizing them by subsequent suspension polymerization. SPG (Shirasu porous glass) membrane was employed to form uniform size droplets having the coefficient of variation (CV) around 10%. Styrene (ST) and acrylic monomers were used as monomers, and their polymers were dissolved in the droplets to investigate the development of phase separation. When hydrophilic methyl methacrylate (MMA) was polymerized in the droplets with a mixed solvent consisting of hydrophilic hexanol (HA) and hydrophobic benzene and hexadecane (HD), the resulting morphology shifted from hemisphere to sandwich and eventually to PMMA/solvent core-shell with increasing hydrophilicity of the mixed solvent. The sandwich was converted to the core-shell after several weeks elapsed. As styrene was added to MMA, the morphology shifted from hemisphere core/solvent shell to raspberry core/solvent shell as the fraction of ST increased. The domain of the mixed solvent in the raspberry core was reduced with increasing the hydrophilicity of the mixed solvent. All these morphologies were eventually converted to the copolymer core/solvent shell. When a mixed monomer of styrene and MMA dissolving polystyrene (PS) was polymerized, the resulting morphology shifted from salami to core-shell with increasing the MMA fraction in the comonomer. The salami particles were then swollen with toluene, and after the swelling, toluene was removed under the different temperature and pressure. The final particle morphology converted to the core-shell with a milder rate of toluene removal which was predicted from the thermodynamic model. When styrene and cyclohexyl acrylate (CHA), a pair with widely different reactivity ratios, were copolymerized, salami morphologies, with tiny CHA-rich domains dispersed in the matrix, were obtained even at a higher fraction of CHA in comonomer. Effects of glass transition temperature of the polymers, molecular weight, and the composition of copolymers were taken in consideration whenever the final morphologies were discussed. By these experiments, the authors tried to demonstrate an advantage of using large uniform spheres for the particle morphology studies. SPG emulsification technique was a potential tool because of its free formulation of the droplets, and the subsequent polymerization could undergo without the breakup or coalescence of the droplets. © 2001 John Wiley & Sons, Inc. J Appl Polym Sci 79: 2200–2220, 2001

Correspondence to: S. Omi.

Journal of Applied Polymer Science, Vol. 79, 2200–2220 (2001)

Key words: SPG (Shirasu Porous Glass) membrane; particle morphology; emulsification; suspension polymerization; styrene; acrylates

INTRODUCTION

Investigations of the particle morphology and the process of morphology development are quite interesting subjects for the researchers working in the field of polymer colloids. Since the particle morphology of synthesized latex is directly related to the properties of films and cast products, its prediction and controlling are utmost importance for determining the recipe and designing operation of polymerization.

There have been two major approaches to investigate the particle morphologies. One is rather straightforward, a methodology to obtain a clear visual image of the morphology. Direct observations by scanning electron microscopy (SEM) and transmission electron microscopy (TEM) have further progressed by an introduction of the staining technique. An ultra-thin microtomed section of the particles, which is prepared by embedding dried particles in epoxy resins, is stained with volatile rare metal oxides such as OsO_4 and RuO_4. In principle, these tetroxides react with specific functional groups in the polymer chains and deflect the electron beam, revealing a particular domain where the reaction took place. Osmium tetroxide is well known to react with double bonds and yield sin-diol. Polybutadiene and its copolymers, which possess residual double bonds, can be stained with OsO_4. Vitali and Montani[1] pointed out that the low diffusion of OsO_4 in polymer often results in a poor contrast between the phases, leading to the less precise determinations.

Ruthenium tetroxide is more reactive and stains various polymers such as polystyrene (PST), polyvinyl acetate, polyvinyl alcohol (PVA), and even some of polyolefins, but barely stains polymethyl methacrylate (PMMA) and other acrylate polymers. Trent et al.[2] provided a comprehensive list of polymers stainable with RuO_4. Vanderhoff[3] introduced the background staining with phosphotungstic acid (PTA), which selectively stains the matrix (background) resins. Unstainable PMMA phase looms up as a white domain when the background staining technique is employed with a combination of the direct staining. Uranium acetate had been used for the same purpose. SEM also provides a clear particle morphology by the etching process, in which the skin layer of polymer particles were selectively washed out with good solvents.[4]

Whereas electron microscopy offers us an integrated view of the particle morphology, various spectroscopic techniques probe the local morphology in polymer particles, particularly at the interphase. Ottewill and coworkers[5] established the short-angle neutron scattering (SANS) technique which, in principle, detects deuterium-labeled polymer chains in the particles.

Neutrons transmit through the hydrogen atom, however, they are scattered by deuterium atoms. Mathematical analysis will transform the scattering pattern into the real image. Winnik and coworkers[6] incorporated fluorescent probes (aromatic compounds such as anthracene, phenanthrene, and naphthalene) in the side-chains of monomers and detected the location of these probes in the particles by the direct energy transfer and quenching process. The real advantage of these spectroscopic techniques is that not only they provide information at the interphase such as core/shell structure, but also they can accurately locate a particular deuterated species. For example, SANS can determine whether polymeric stabilizers (poly-12-hydroxystearic acid) are extend toward the continuous medium or they are collapsed on the polymer surface in nonaqueous phase dispersion polymerization.[7] Landfester et al.[8] showed that the solid state (^1H and ^{13}C) NMR could provide the information about soft-core/hard-shell interphase by way of the spin diffusion measurements. The detection of components on the surface can be done by the classical surfactant titration[9] or recent XPS(ESCA) spectroscopy.[10] Recently, comprehensive books of the particle morphology have been published together with the advanced characterization principles and techniques.[11,12]

The theoretical prediction of particle morphology has been also extensively studied, at first based on the theory of thermodynamics, and recently by more dynamic mathematical modeling.

The thermodynamic approach answers the question why one particular type of morphology prevails to the others. The thermodynamically preferred equilibrium morphology of a particle under the state of complete phase separation is the one which is formed with a minimum total free energy change from the initial state. It is

generally accepted that the free energy change is correctly estimated from the summing up of interfacial energies corresponding to the newly created interfaces after the final morphology developed. This can be clearly stated in the following equation:

$$\Delta G = \sum \gamma_{ij} A_{ij} - \gamma_0 A_0 \quad (1)$$

where ΔG is total free energy change, γ_{ij} and A_{ij} = interfacial tension and area between the components i and j, γ_0 and A_0 are interfacial tension and area between the initial particle (or droplet) suspended in the continuous phase and the continuous phase, respectively. Normally, aqueous phase is selected as the continuous phase. Interfacial tensions between any two phases can be determined experimentally, or some of them may be available from the literature.

However, one of the idealized model geometries should be fitted to the real particle morphology in order to know A_{ij} before calculating ΔG from eq. (1). A reduced form of free energy change has been preferred to do this kind of analysis, and can be written

$$\Delta\gamma = \sum \gamma_{ij}(A_{ij}/A_0) - \gamma_0 \quad (2)$$

Sundberg et al.[13] and Chen et al.[14] proposed a set of model composite particles, the interfacial areas of which can be derived from geometrical algebra, and compared the observed particle morphologies with the thermodynamically probable ones in their two component systems, seed polymerizations of polystyrene, PS/MMA, and PMMA/styrene, and some artificial lattices by solvent evaporation. Sundberg and Sundberg[15] extended this approach to three component systems, derived the mathematical expressions of for 22 possible model morphologies of the composite particles. Some of those morphologies were observed in their experiment of three-component artificial latices.

In the actual polymerization process, the final attainment of the particles to the thermodynamically favored morphology is prevented by several kinetic factors in the later stage of polymerization such as slow diffusion rate of polymer chains, and viscosity buildup. Asua and coworkers[16] proposed a complicated kinetic model that took account of the mass-transfer rate of clusters of the one polymer domain moving through the matrix of the other polymer, as well as the progress of polymerization, which led to the increasing viscosity in the particle.

The present authors have been working with the preparation of uniform polymeric microspheres (from a few μm to 100 μm) by using a particular glass membrane [Shirasu porous glass (SPG)] emulsification technique and the subsequent suspension polymerization or solvent evaporation process.[17–20] The uniformity in size of the droplets obtained by the emulsification process was retained during the later preparation stages. While doing these experiments, we have observed various kinds of particle morphologies, one-eyed, blood cell (collapsed sphere), and hollow particles. Having been aware that the uniform droplets (and the particles obtained after the above treatments) offer clear visual images of morphologies, we published our own morphology studies related to the preparation of polylactide particles[21] and artificial composite latex of PS–PMMA.[22] Sundberg and Sundberg's theoretical expressions, which were limited to the equi-volume three component system, were extended to the system available for arbitrary compositions.[23] These morphologies were all thermodynamically favored, obtained from a very slow evaporation of the solvent. Then, our interest was shifted to the observation of kinetically controlled morphologies. This article presents the morphology developments of the polymer particles, starting from the homogeneous droplets consisting of monomers, polymer, good and poor solvents, and initiator.

First, the droplets composed of styrene/MMA comonomer and a mixed solvent, benzene, hexadecane (HD), and hexanol (HA) were polymerized in order to investigate the behavior of mobile components (solvents) in the polymer particles. Second, polystyrene was dissolved in the comonomer of styrene/MMA, and the droplets were polymerized to compare the extent of phase separation depending on the composition of comonomer and also to investigate the effect of hydrophilicity of polymers (PMMA and MMA copolymer), a driving force for polymer chains moving to the interface. Swelling of the final polymer particles with toluene followed by its evaporation under different temperature and reduced pressure was also tried to confirm that the kinetically controlled morphology can be converted to the thermodynamically favored one when the components are allowed to be mobile in the particle. Finally, a monomer pair, styrene and cyclohexyl acrylate (CHA), which has widely different reactivity ratios, were copolymer-

ized to detect any inhomogeneity caused by the possibly broad drift of copolymer composition.

EXPERIMENTAL

Reagent

All the reagents were purchased from Kishida Chemical Co. unless stated otherwise.

Monomer

Styrene and MMA were all distilled under reduced pressure to remove inhibitor and were stored in a refrigerator until use. CHA was washed with 3 wt % sodium carbonate solution three times, washed with the distilled-deionized water (DDI) five times and dried with a 4-Å molecular sieve. The dried CHA was stored in a refrigerator until use.

Initiator

Benzoyl peroxide (with 25 wt % moisture) (BPO) and 2,2′-azobis(2,4-dimethylvaleronitrile (V-65, ADVN, Wako Pure Chemical Co.) were reagent grade and were used as received.

Inhibitor

Water-soluble inhibitor was added in the aqueous phase in order to prevent the secondary nucleation of polymer particles. Hydroquinone (HQ) and sodium nitrite were reagent grade and was used as received.

Stabilizer and Surfactant

Polyvinyl alcohol (degree of polymerization = 1700, 88% hydrolyzed, PVA-217, Kuraray) was used as received. Sodium lauryl sulfate (SLS, Merck) was biochemistry grade and was used as received.

Solvent

Benzene (Bz), toluene (Tol), hexadecane (HD), and hexanol (HA) were reagent grade and were used as received.

Others

Sodium sulfate (Kokusan Chemical Co.) was commercial grade and used as received.

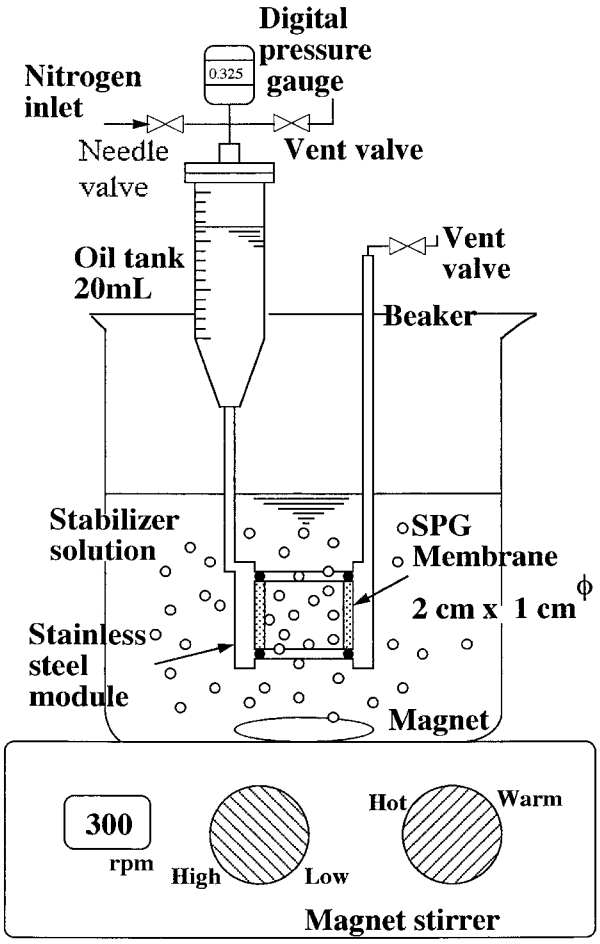

Figure 1 Schematic diagram of Shirasu porous glass (SPG) membrane emulsification kit.

Procedure

Emulsification

A schematic diagram of the SPG emulsification apparatus (Kiyomoto Iron Co.) is shown in Figure 1. An SPG membrane cylinder, 1cm outer diameter and 2-cm length with 1.42-μm pore size (Ise Chemical Co.), was installed in a stainless steel module. A 20-mL Teflon oil tank and an air vent were attached, and the whole kit was immersed in the aqueous solution dissolving PVA, SLS, sodium sulfate, and the water-soluble inhibitor.

The oil phase was poured in the oil tank and the top of the tank was connected to the nitrogen supply line. The nitrogen gas pressure was carefully controlled with a Nupro needle valve and monitored by a three-digit pressure gauge. The oil phase was pushed through the pore, and if the applied pressure was adequate, uniform droplets were released steadily from the pores. A gentle

circulation of the aqueous phase maintained the droplets in stable dispersion without creaming, coalescence, and breakup, After the emulsification, the emulsion was transferred to the reactor for the swelling of hydrophilic components or for direct polymerization.

In some experiments, another SPG emulsification apparatus, a larger capacity with the membrane of 17-cm length, was used.[24]

Swelling

Since the fabric of SPG membrane is Al_2O_3–SiO_2, hydrophilic components such as MMA and hexanol are apt to wet the membrane surface. When hydrophilic components were dominant in the formulation of oil phase, only the hydrophobic components were emulsified with the membrane emulsification process, and the hydrophilic ones were impregnated in the hydrophobic (seed) droplets by swelling. The hydrophilic oil phase was emulsified with a twice volume of distilled and deionized (DDI) water dissolving a small amount of SLS by using a homogenizer (Hi-Flex Homogenizer HF93, SMT Co.) with 10,000 min^{-1} for 10 min (secondary emulsion). The emulsion was transferred to the reactor containing the seed emulsion, and the mixture was allowed to stand with an agitation rate of 160 min^{-1} until the smaller droplets of the secondary emulsion disappeared.[25]

Polymerization

A 500-mL four-necked glass flask was used as a reactor. A nitrogen inlet tube, a condenser with a nitrogen outlet tube attached, and a stirrer with a half-moon-shaped blade, were equipped. The nitrogen was bubbled gently in the emulsion (while the swelling process continued) to remove the dissolved oxygen. After one hour or the swelling was over, the temperature was raised to 343 K, and the emulsion was polymerized for 24 h.

Analyses

Monomer Conversion

After the polymerization, the latex was well mixed, and a certain amount was precisely weighed. The polymer was precipitated by adding an adequate amount of methanol, washed several times with methanol, separated from the serum by centrifuge, and dried in a vacuum oven. The dried weight was measured, and the monomer conversion was calculated in the normal way. When polymer was dissolved in the initial oil phase formulation, run 5814, 5816, and 5817 as shown later, the contribution of the polymer weight was subtracted from the dried weight. The dried particles served for the measurement of molecular weight and for the preparation of samples for TEM observations.

Microscopy

An optical microscope (OM) (BHC-313, Olympus), a SEM (JSM-5300, JEOL), and a TEM (H-700H, Hitachi) were used for the visual observation of particle morphologies. OM was useful for the observation of initial droplets and the final particles having the separated solvent domains.

SEM samples were prepared by dropping a few latex droplets diluted by 1000-fold in DDI water on a brass sample rod covered with aluminum foil and dried in a desiccator for more than 24 h. The gold was then spattered with a vacuum coater (JFC-1200, Fine coater, JEOL). The acceleration voltage of electron beam was fixed at 15 kV.

Ultra-microtomed and RuO_4-stained samples for TEM observation were prepared by mixing the dried polymer particles with epoxy resin, put the mixture in gelatin capsules, and dried them overnight. The hardened resin was ultra-thin sliced with a glass knife equipped in a microtome (MT-7000, Microtome, RMC), and the sliced sample was scooped up on a copper mesh disk covered with carbon-spattered collodion film, dried overnight, and exposed to the atmosphere of 0.5% (wt) RuO_4 solution for 90 min. The acceleration voltage of electron beam was fixed at 175 kV.

Molecular Weight

Average molecular weights and molecular weight distribution of the polymer fractions soluble in tetrahydrofuran (THF) were measured with a GPC (HIC 8020, Tohso Co.). Insoluble and gel portions were removed by the filtration with 0.45-μm Teflon membrane filter. Standard PS samples were used for calibration.

Thermal Analysis

Glass transition temperatures and other thermal behaviors were observed with a DSC (DSC-3100, MacScience Co.). The sample was scanned twice in order to eliminate the disturbances (e.g., moisture, volatile solvents, void space in the sample) that may have been detected in the first scan.

Table I Formulation for Solvent–Monomer Emulsion (in grams)

	Run No.								
Ingredients	5809	5810	5811	5849	5850	5851	5844	5845	5846
Styrene	0	0	0	11.25	11.25	11.25	22.5	22.5	22.5
MMA	22.5	22.5	22.5	11.25	11.25	11.25	0	0	0
Benzene	19.5	19.5	19.5	19.5	19.5	19.5	19.5	19.5	19.5
Hexadecane	4.0	4.0	4.0	4.0	4.0	4.0	4.0	4.0	4.0
Hexanol	7.5	15.0	22.5	7.5	15.0	22.5	7.5	15.0	22.5
BPO	0.84	0.84	0.84	0.84	0.84	0.84	0.84	0.84	0.84
DDI water[a]	295	295	295	295	295	295	295	295	295
PVA	1.5	1.5	1.5	1.5	1.5	1.5	1.5	1.5	1.5
SLS[a]	0.045	0.045	0.045	0.045	0.045	0.045	0.045	0.045	0.045
Na_2SO_4	0.05	0.05	0.05	0.05	0.05	0.05	0.05	0.05	0.05
$NaNO_2$	0.02	0.02	0.02	0.02	0.02	0.02	—	—	—
Hydroquinone	—	—	—	—	—	—	0.02	0.02	0.02

MMA, methyl methacrylate; BPO, benzoyl peroxide; DDI, distilled and deionized; PVA, polyvinyl alcohol; SLS, sodium lauryl sulfate.

[a] 225 g of DDI water and 0.025 g of SLS were used for the primary emulsion. 70 g of DDI water and 0.02 g of SLS were used for the secondary emulsion.

Surface and Interfacial Tension

Surface tensions of the aqueous phase and the oil phase (mixture of monomers, solvents and other additives), and the interfacial tensions between them were measured by a DeNouy surface tensiometer. Interfacial tensions between polymers and the above liquids were calculated from contact angles measured with a contact angle meter (FACE contact angle meter, CA-D type, Kyowa Interface Science Co.).

The sample polymer film was prepared by dissolving the polymer in chloroform, cast the solution on a glass plate, and the solvent was evaporated. The interfacial tension was calculated from the following equation:

$$\gamma_{S-L} = \gamma_S - \gamma_L \cos\,\theta \qquad (3)$$

where $\gamma S\text{-}L$, γS, γL is interfacial tension between polymer and liquid, surface tension of polymer and liquid, respectively, and θ is the contact angle between polymer and liquid.

RESULTS AND DISCUSSION

PMMA, P(MMA–co-styrene, 1:1) and PS/Solvent Polymer Particles

Among a number of factors controlling the particle morphology, the mobility and the hydrophilicity of the component are singularly important because the latter will decide the thermodynamically favored location of the component, whereas the former will promote the establishment of equilibrium morphology.

The effects of inert, smaller molecules to the particle morphology developments of PMMA, P(MMA–co-styrene, 1:1) and PS were investigated by changing the composition of mixed solvent composed of benzene, hexadecane and hexanol. Benzene and HD are hydrophobic, whereas HA is hydrophilic. Their solubility in water at room temperature is reported as 0.59 wt % for HA, 0.171 wt % for benzene, and $9(10^{-8})$ wt % for HD[18,26]), respectively. By contrast, benzene is a good solvent for the polymers, while the other two are poor solvents. The solubility parameter of benzene is reported as 9.2 $(\text{cal/cm}^3)^{1/2}$, 10.7 for HA, and 7.9 for HD, respectively,[18,26] whereas it is 9.1 for PS, and 9.3 for PMMA.[27] In the following experiments, the amount of the hydrophobic solvents were fixed, and only the amount of HA was changed to adjust the hydrophilicity of the mixed solvent. In this way, two-dimensional experiments, one axis representing the relative hydrophilicity of mobile components and the other, that of slowly moving polymers, were carried out. The detailed formulation of the oil phase is shown in Table I. The primary emulsion was prepared only with the hydrophobic components in the oil

phase, and later hydrophilic MMA and HA were absorbed by the swelling process.[25,26]

OM photographs of the polymer particles suspended in the aqueous phase are shown in Figure 2, and SEM photographs of the solvent-free, dried particles are shown in Figure 3. Average diameters of the droplets in the primary and the swollen emulsions, and those of the polymer particles after the polymerization are listed in Table II together with the final solid content in the latex and the average molecular weights. As shown in the footnotes to Table II, ds_{calc} and dp_{calc} can be derived as follows, assuming that the swelling of MMA and HA was complete, and 100% monomer conversion was attained:

$$\bar{d}_{s,\mathrm{calc}} = \bar{d}_e \left(\frac{\text{total weight of oil phase}}{\text{total weight of hydrophobic components}} \right)^{1/3} \quad (4)$$

$$\bar{d}_{p,\mathrm{calc}} = \bar{d}_{s,\mathrm{calc}} \left(\frac{\text{total weight of monomers}}{\text{total weight of oil phase}} \right)^{1/3} \quad (5)$$

The density difference between the total oil phase and the hydrophobic components can be neglected in eq. (4). The volume contraction due to the polymerization was neglected in eq. (5).

The primary emulsions (seeds) of the later two series of experiment, run 5849–5851 and run 5844–5846, were prepared in one batch, using an SPG apparatus of larger capacity.[24] Those of the first series, run 5809–5811, were prepared separately, using the apparatus in Figure 1.

Observation of Particle Morphology From OM and SEM Photographs

From the first row in Figure 2 (OM photographs), one could notice that the morphology of PMMA spheres shifted from hemisphere to sandwich, and eventually to core-shell with increasing the hydrophilicity of the mixed solvent, in other words, as the composition of HA in the solvent increased. This tendency is understandable, the hydrophilicity of PMMA was at first comparable with that of the mixed solvent, and was finally overcome in run 5811. Note that all the surfaces of dried particles are smooth as shown in Figure 3 (SEM photographs).

The photographs of the middle and third row in Figure 2 show unanimous core-shell type morphologies, although the shell in Figure 2(d) (run 5849) is difficult to recognize. This implies that the copolymer became hydrophobic even though compared with the most hydrophobic mixed solvent in run 5849.

SEM photographs in the middle row of Figure 3 show the three phase morphologies for all the runs, core-shell (or possibly a slight hemisphere) with a pinhole core (run 5849), core-shell with an acorn-like core (run 5850), and core-shell with a golf ball core (run 5851), respectively. The pinholes on the surface in Figure 3(d) are recognizable only by a careful inspection compared with those in Figure 3(f). These figures and those in the last row show that the solvent phase was also separated in two domains.

In the last row, the morphologies of the most hydrophobic PS particles were similar to those of the middle row except that the phase separation between the polymer and the solvent phase was more enhanced. The cores of the first two columns (runs 5844 and 5845) are mixtures of the two types of morphologies—hemisphere and golf ball—whereas the last column (run 5846) returned to golf ball core, the holes becoming larger than those of run 5851.

Besides the major factor to determine the particle morphology which is the hydrophilicity of the component, the second factor appeared in run 5849–5851 and run 5844–5846, that is the miscibility between the solvents, including the unreacted monomers. As the polymerization progressed, the poor solvents (HA+HD) started to separate from the polymer phase composed of polymer, monomer, and benzene, admitting that the partitions of the components between the two phases should be taken into account. For the sake of simplicity, and because we have no available photographs or data to verify, the partitions are only speculative in the following discussions. The most hydrophilic HA will be diffusing out to the interface, whereas the most hydrophobic HD will tend to remain inside the droplets unless enough amount of HA is present and drags HD together as a solute. The big hole present in each polymer particle in runs 5844 and 5845 indicates the trace of HD-rich domain separated from the HA-rich phase and also from PS, whereas the smaller traces are those of HD partitioned in the HA phase, which separated in the later stage of polymerization. Apparently more hydrophilic PMMA surface (run 5810) expelled HD to the HA phase; i.e., HD was present in the HA phase either in tiny domains or in dissolved state. That the size of tiny dents (holes) increased with increasing hydrophobicity of the particle surface (the last col-

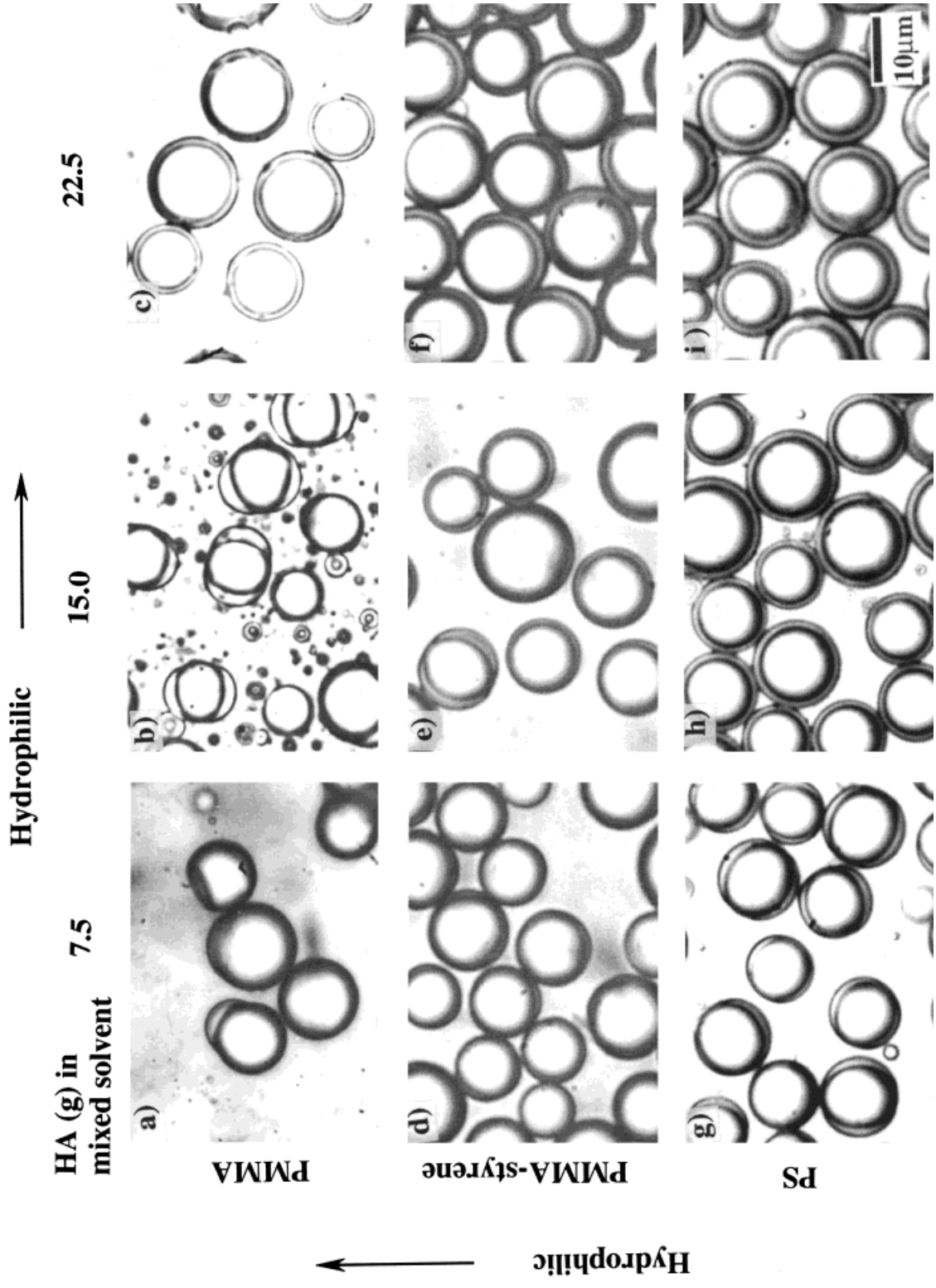

Figure 2 Optical photographs of latex particles showing two-dimensional morphology change with hydrophilicity of polymer and the mixed solvent. (a) Run 5809. (b) Run 5810. (c) Run 5811. (d) Run 5849. (e) Run 5850. (f) Run 5851. (g) Run 5844. (h) Run 5845. (i) Run 5846.

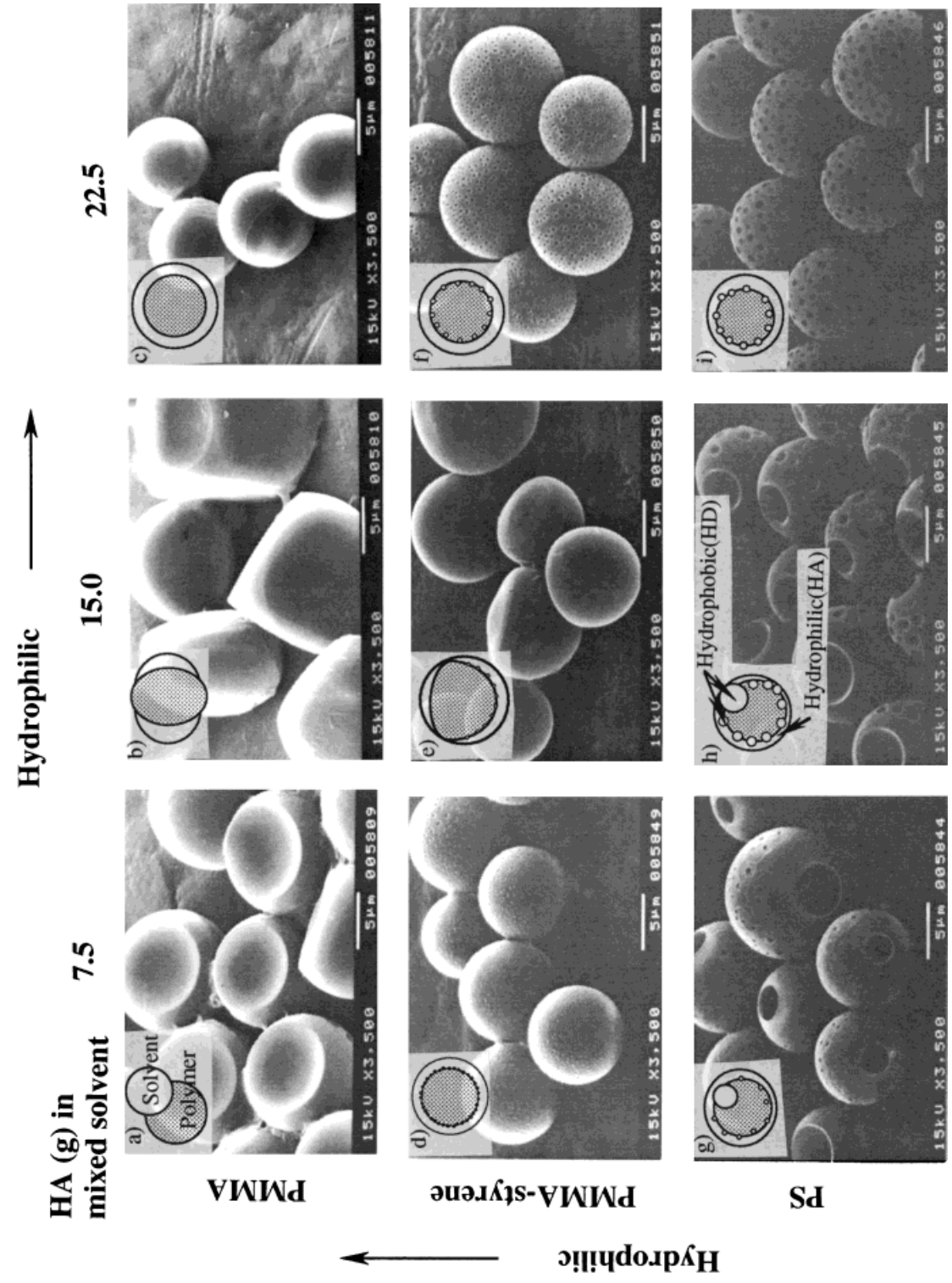

Figure 3 SEM photographs of dried polymer particles showing two-dimensional morphology change with hydrophilicity of polymer and the mixed solvent. (a) Run 5809. (b) Run 5810. (c) Run 5811. (d) Run 5849. (e) Run 5850. (f) Run 5851. (g) Run 5844. (h) Run 5845. (i) Run 5846.

Table II Experimental Results of PMMA, P(MMA-Co-Styrene, 1 : 1), PS/Solvent Particles

	Run Number								
	5809	5810	5811	5849	5850	5851	5844	5845	5846
d_e (μm)	11.5	9.66	9.12	11.0	11.0	11.0	10.2	10.2	10.2
CV (%)	12.5	14.2	16.2	11.7	11.7	11.7	14.3	14.3	14.3
$d_{s,\mathrm{obs}}$ (μm)	14.8	11.5	14.7	13.3	13.8	14.5	12.5	13.1	13.9
CV (%)	13.2	11.8	15.0	10.4	10.8	11.8	11.4	12.3	12.4
$d_{s,\mathrm{calc}}$ (μm)	13.1	13.2	12.9	12.7	13.2	13.7	10.7	11.2	11.6
$d_{p,\mathrm{obs}}$ (μm)	12.0	Sandwich	11.1	9.46	9.01	9.20	9.36	9.80	9.14
CV (%)	12.9	—	26.2	14.7	12.0	12.2	14.0	15.0	14.6
$d_{p,\mathrm{calc}}$ (μm)	9.17	9.43	8.87	9.47	9.43	9.42	7.98	8.00	7.97
Monomer conversion (%)	63.8	68.7	37.2	83.7	84.7	81.2	91.2	87.8	73.2
Mol. wt.									
$M_n(\times 10^{-4})$	2.38	1.93	1.52	0.897	1.16	1.25	1.04	0.816	0.902
$M_w(\times 10^{-4})$	6.81	5.53	5.26	2.07	2.27	2.44	2.16	1.90	1.89
M_w/M_n	2.86	2.87	3.45	2.3	1.85	1.96	2.09	2.33	2.10

CV, coefficient of variation.
d_e = average diameter of primary emulsion droplets (hydrophobic).
$d_{s,\mathrm{obs}}$ = average diameter of swollen droplets.
$d_{p,\mathrm{obs}}$ = average diameter of dried polymer particles assumed as spherical shape.

$$\bar{d}_{s,\mathrm{calc}} = \bar{d}_e\left(\frac{\text{total weight of oil phase}}{\text{total weight of hydrophobic components}}\right)^{1/3}$$

$$\bar{d}_{p,\mathrm{calc}} = \bar{d}_{s,\mathrm{calc}}\left(\frac{\text{total weight of monomers}}{\text{total weight of oil phase}}\right)^{1/3}$$

umn) seems to confirm this argument. Also, although no visual evidence was obtained from Figures 2 and 3, it will not be too farfetched to assume that the shell domains of the particles in runs 5849 and 5850 were separated in the HD-rich and HA-rich domains. Unless separation occurred, the acornlike particles would not have been obtained after drying. This probable phase separation between HA and HD will be discussed again in the next section.

Further Discussion From Table II

All values of the coefficient of variation (CV) for the initial droplets, swollen droplets, and the final polymer particles displayed the reasonable uniformity of the droplets and the particles except the polymer particles of run 5811. Generally, the final monomer conversions, or the solid contents in the latex, were pretty low with the homopolymerization of MMA (run 5809–5811). As the amount of HA increased, the solubility of MMA in the aqueous phase and the provability of radical exit from the droplets became higher. This favored the secondary nucleation of polymer particles despite the presence of the inhibitor ($NaNO_2$) in the aqueous phase. The formation of the smaller particles accelerated coagulation between the droplets, leading to the instability of the system. Run 5811 was mostly affected. The formation of smaller particles was reflected in larger molecular weights and broader distribution compared with the others.

As for the swelling process, the comparisons between $d_{s,\mathrm{obs}}$ and $d_{s,\mathrm{calc}}$ indicated that $d_{s,\mathrm{obs}}$ was generally larger than $d_{s,\mathrm{calc}}$, implying that a minor coalescence between the seed droplets may have occurred during the swelling period. As all the values of CV remained at around 10%, the possible coalescence did not seriously affect the later morphology development.

Comparison between $d_{p,\mathrm{obs}}$ and $d_{p,\mathrm{calc}}$ suggested that a reasonable amount of the solvents (rich in benzene and probably HA as well) still remained in the PMMA particles (run 5909–5811). The same tendency, $d_{p,\mathrm{obs}} > d_{p,\mathrm{calc}}$, had been observed in our first synthesis of PMMA spheres accompanied with the droplet swelling.[25] Another reason was that the volume of the spheres was overestimated due to the inclusion of hole volumes on the surface of the PS particles (run 5844–5846).

Equilibrium Morphologies of the Solvent–Polymer Particles

Except for the hemisphere morphology as shown in Figures 2(a) and 3(a) (run 5809), all the other morphologies observed immediately after the

polymerization were converted to the polymer–core/solvent–shell morphology after a couple of weeks or months. All the dents and big hole on the particle surface disappeared, and the mixed solvent phase was homogeneous, as far as the OM observations revealed. As we did not expect these dramatic shifts of morphology, how the precise time required to attain the equilibrium state depended on the composition of the droplets was unclear.

Because of the remnant of benzene, unreacted monomers, and probably HA in the polymer phase, the polymer chains of high glass transition temperatures (373 K for PS and 378 K for PMMA) were still mobile, allowing a gradual rearrangement of the components.

Although the detailed plots are not shown here, the thermodynamic theory based on the calculation by employing eq. (2) favored the polymer–core/solvent–shell morphology to be a first possibility for all the runs listed in Table I. The next possibility was the hemisphere, and the separated state of droplet and particle followed pretty closely in two cases, P(MMA–co- styrene, 1:1) and PS. The inverted core-shell was a remote possibility. The difference between the core-shell and the hemisphere for run 5809 was approximately 4 mN/m. The employed data of surface and interfacial tensions are shown in Table A-I for future use.

Morphology Development With the Progress of Polymerization

The morphology development with the progress of the polymerization was investigated by selecting the formulation employed for run 5810. Run 5810 yielded a sandwich-type morphology, as shown in Figures 2(b) and 3(b). A series of OM photographs showing the morphology development during the polymerization, from droplets to particles, are shown in Figure 4. The progress of polymerization is shown in Figure 5 as the time-dependent plots of monomer conversion and number average molecular weight.

As Yuyama et al.[28] reported in their suspension polymerization of styrene-HD-benzoyl peroxide (BPO) droplets, the phase separation was already observed after 2 h with 30% monomer conversion, as shown in Figure 4(a) (although not so clear from the photo because of exposure to the light beam). Two sandwichlike broader domains of the mixed solvent were distinguishably clear after 5 h with 70% monomer conversion together with the smaller circular domains [Fig. 4(b)]. These smaller domains were gradually absorbed in the broad domains [8 h, 80% conversion, Fig. 4(c)], and disappeared completely after 24 h [Fig. 4(d)]. Note that the polymerization seemed to be stalled around at 80% monomer conversion after 8 h from the plots in Figure 5 (molecular weight also ceased to decrease), whereas the development of the sandwichlike morphology still continued. This confirms that the smaller species such as the solvents and monomers are still mobile enough, even though the viscosity in the polymer phase became very high.

This experiment demonstrates the value of SPG emulsification technique for particle morphology investigation because of the stable droplets, easier sampling, and straightforward observation of the morphology.

PMMA–PS Composite

In order to investigate the effect of the inert polymer chains dissolved in the monomer phase to the final particle morphology, polystyrene (M_n = 7600, M_w = 16900, M_w/M_n = 2.22) was dissolved in MMA or the mixture of MMA and styrene, and the polymerization was carried out. The experimental formulation for each run is shown in Table III, and the results of emulsification and polymerization are shown in Table IV.

Particle Morphology

All the polymer particles obtained in each run remained spherical from the SEM observation without any noticeable feature on the surface. Then, the microtomed section of the polymer particles were stained with the vapor of RuO_4 and observed with TEM. The TEM photographs are shown in Figure 6. With increasing composition of MMA in the comonomer, the particle morphology shifted from salami-type (runs 5814 and 5816) to core (salami)-shell (run 5817).

The dark-stained domains of PS grew in size because the compatibility between PS and the newly formed P(MMA–co-styrene) became less favorable due to the decreased fraction of styrene in the copolymer chains. When MMA was homopolymerized in run 5817, eventually a core-shell morphology was attained. However, there are some PMMA domains remained in PS core that suggested the morphology was partially kinetically controlled. To verify this speculation,

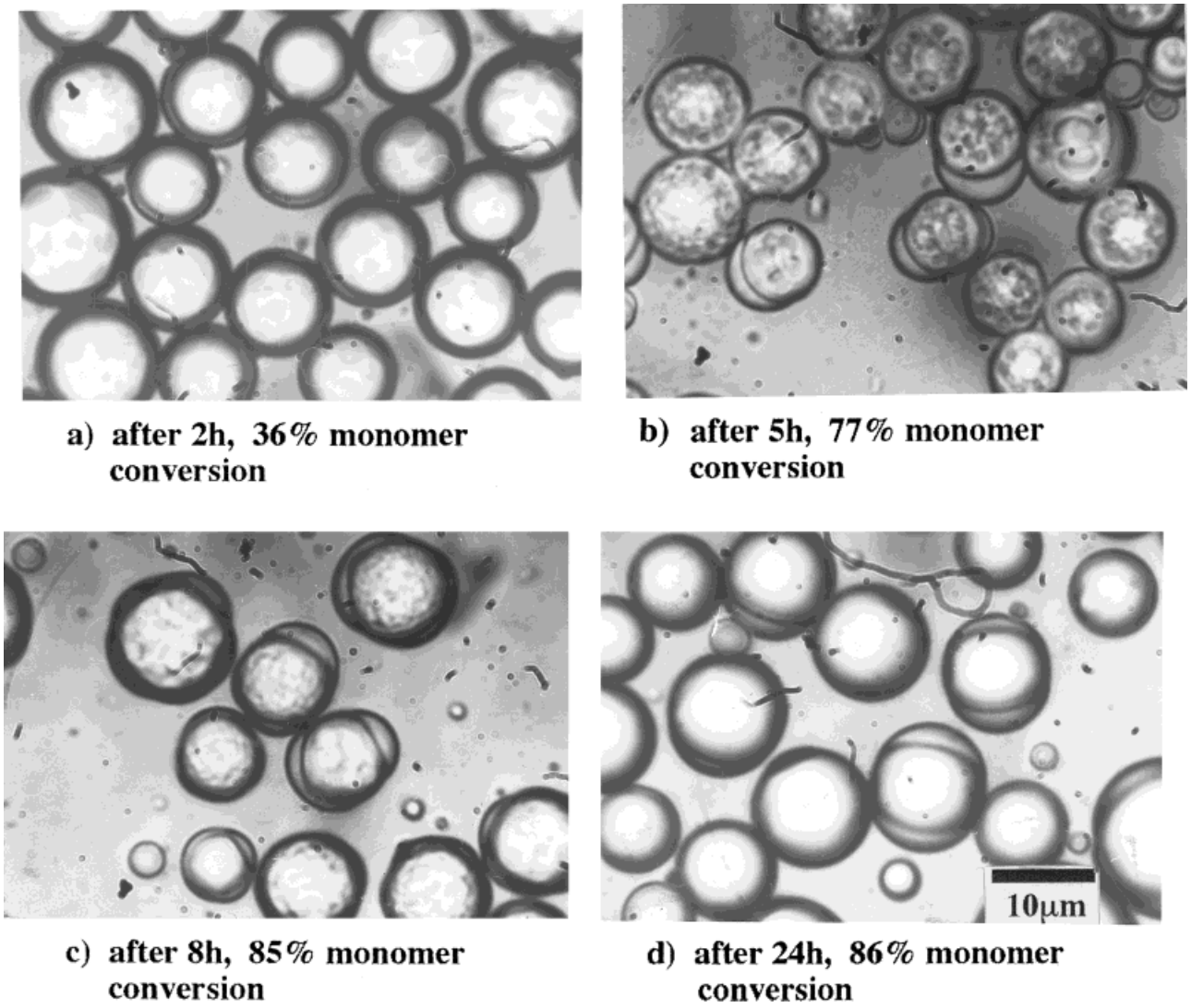

Figure 4 Development of phase separation in polymer particles during the polymerization. Run 5810.

thermodynamically favored morphology was determined from the calculation by using eq. (2).

Calculated values of the change of reduced free energy ($\Delta\gamma$) was plotted in Figure 7 against the axis of the interfacial tension between P(MMA–co-styrene) and the aqueous phase, the plot range covers an entire copolymer composition (see the interfacial tension data in Table A-I). It can be seen that the core-shell morphology is most favored in every run.

Discussion of Results Summarized in Table IV

Before the further investigation concerned with the thermodynamically favored morphology in this experimental system, the observed and calculated data in Table IV should be examined. Since no inert additives were added in the oil phase, the equations to obtain $d_{s,\mathrm{calc}}$ and $d_{p,\mathrm{calc}}$ should be modified as follows:

$$\bar{d}_{s,\mathrm{calc}} = \bar{d}_e \left(\frac{\text{total weight of oil phase}}{\text{total weight of oil phase in primary emulsion}} \right)^{1/3} \quad (6)$$

$$\bar{d}_{p,\mathrm{calc}} \cong \bar{d}_{s,\mathrm{calc}} \quad (7)$$

As no hydrophobic HD was added in the oil phase in order to avoid the further complexity that might arise from adding the third component to

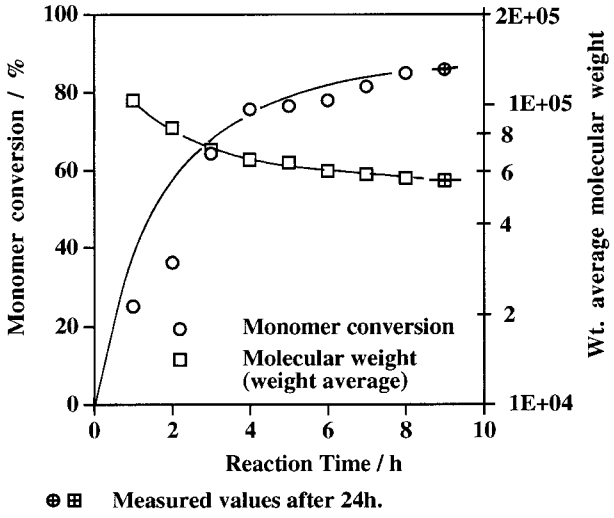

Figure 5 Monomer conversion and weight average molecular weight plotted against elapsed time. Run 5810.

the PS–comonomer system, the hydrophilicity of MMA was not limited, which led to the undesirable wide distribution of the droplets. Both the average droplet size and its higher CV, and the molecular weight and its broadening distribution implied that a substantial amount of MMA escaped from the droplets into the aqueous phase, and secondary nucleation took place to a considerable degree in the earlier stage of polymerization. All $d_{s,\mathrm{obs}}$ were smaller than $d_{s,\mathrm{calc}}$ and the average molecular weight increased remarkably with broader distributions, indicating the contribution from the emulsion polymerization. Although most of the escaped radicals were deactivated by $\cdot NO$ or $\cdot NO_2$ radicals generated from sodium nitrite,[29] some still survived and underwent the secondary nucleation. The low final monomer conversions suggest that the polymerization was restricted in the final stage because of the enhanced glassy state in the droplets. For unspecified reasons, run 5816, an intermediate MMA feed, demonstrated the low escape of MMA into the aqueous phase (the largest $d_{p,\mathrm{obs}}$) and the most effective inhibition in the droplets by sodium nitrite (the lowest final monomer conversion and molecular weights).

Table III Formulation for PS-MMA/Styrene Emulsion (in grams)

	Run No.		
Ingredients	5814	5816	5817
PS	2.0	2.0	2.0
MMA	10.0	14.0	18.0
Styrene	8.0	4.0	0
ADVN	0.9	0.9	0.9
Water	180	180	180
PVA	1.0	1.0	1.0
SLS	0.027	0.027	0.027
Na_2SO_4	0.033	0.033	0.033
$NaNO_2$	0.013	0.013	0.013

PS, polystyrene; MMA, methyl methacrylate; ADVN, azobisdimethylvaleronitrile; PVA, polyvinyl alcohol; SLS, sodium lauryl sulfate.

30 g of water dissolving 0.01 g of SLS was used for the preparation of secondary emulsion containing 10 g of MMA. PS was dissolved in 8 g of styrene, styrene/MMA 1 : 1, and MMA in runs 5814, 5816, and 5817, respectively.

Table IV Experimental Results of PMMA/PS Composite Spheres

	Run No.		
	5814	5816	5817
d_e (μm)	8.54	8.52	7.20
CV (%)	9.07	16.5	44.4
$d_{s,\mathrm{obs}}$ (μm)	9.21	9.22	7.99
CV (%)	10.1	16.6	41.0
$d_{s,\mathrm{calc}}$ (μm)	10.6	10.6	8.93
$d_{p,\mathrm{obs}}$ (μm)	7.13	10.0	8.13
CV (%)	9.46	18.6	41.3
$d_{p,\mathrm{calc}}$ (μm)	10.6	10.6	8.93
Monomer conversion (%)	63.3	56.0	71.2
Mol wt			
$M_n(\times 10^{-4})$	5.88	1.17	2.64
$M_w(\times 10^{-4})$	33.0	4.92	15.7
M_w/M_n	5.61	4.22	6.00

CV, coefficient of variation.

$$\bar{d}_{s,\mathrm{calc}} = \bar{d}_e\left(\frac{\text{total weight of oil phase}}{\text{total weight of oil phase in primary emulsion}}\right)^{1/3}$$

$$\bar{d}_{p,\mathrm{calc}} \cong \bar{d}_{s,\mathrm{calc}}$$

Rearrangement of Particle Morphology: Reorientation to Thermodynamically Favored State

In order to prove that the particle morphologies as shown by the stained photos in Figure 6 are, in fact, intermediate ones before settling in the thermodynamically stable state, the polymer particles of run 5816 were swollen with a good solvent, toluene; the solvent was then stripped gradually with a varied intensity of removal. We expected

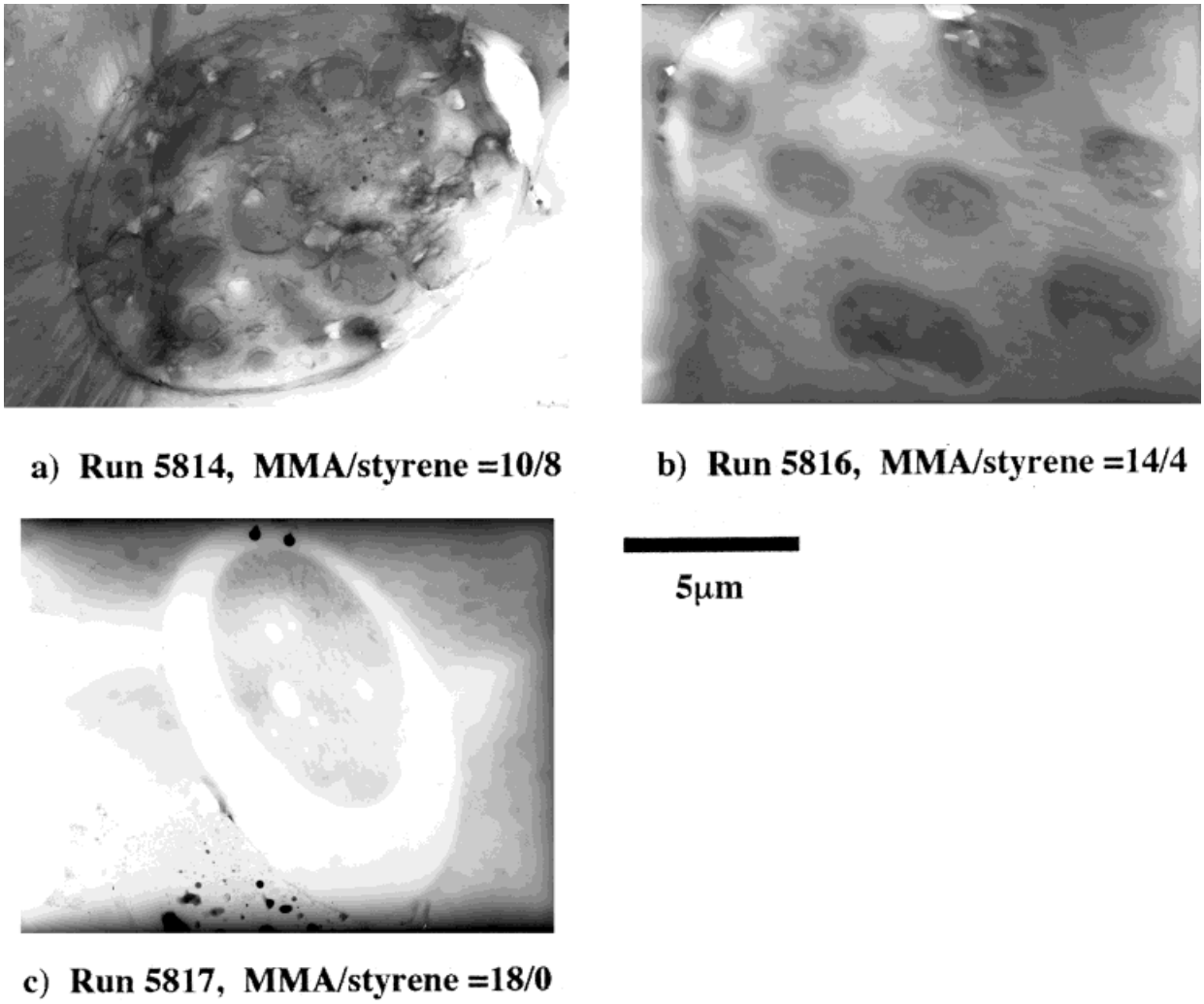

Figure 6 Microtomed and RuO_4-stained TEM photographs of P(MMA–co-styrene)/PS composite polymer particles.

that the polymer chains in frozen state would be mobile again and that they would eventually rearrange to the morphology with a possibly lowest energy level.

A total of 0.907 g of acetone was added to 10 g latex of run 5816 before the addition of 2.79 g of toluene. The presence of acetone in the aqueous phase promoted the transport of toluene from droplets to the polymer particles through the aqueous phase. A preliminary test showed that 1.86 g of toluene was sufficient to eliminate the inhomogeneity in the polymer particles after the swelling of 2 h. OM photographs of the latex before and after the swelling are shown in Figure 8. Note that the inhomogeneity of the polymer particles completely disappeared.

Toluene was stripped under three different conditions. The average diameter of droplets was measured at intervals, and the calculated values of swelling ratios are plotted in Figure 9. The swelling ratio is defined as follows:

$$\text{Swelling ratio} = \left(\frac{\text{average diameter of swollen droplets}}{\text{average diameter of polymer particles}} \right)^3 \quad (8)$$

Regardless of the stripping rate of toluene, the phase separation appeared at the same swelling ratio shown in Figure 10 as a horizontal straight line.

After the stripping, the polymer particles were washed with methanol and dried in a vacuum oven at room temperature. Microtomed samples were stained with RuO_4 vapor and then observed

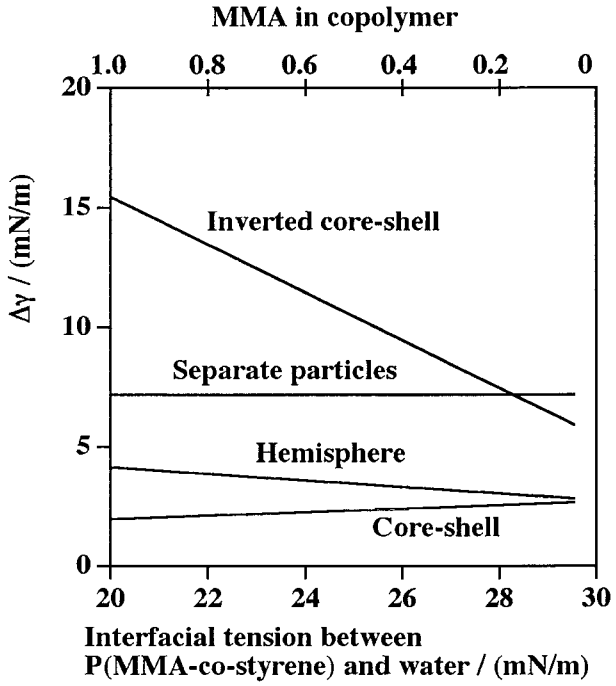

Figure 7 Reduced surface energy ($\Delta\gamma$) of P(MMA–co-styrene)/PS composite polymer particles plotted against interfacial tension between P(MMA–co-styrene) and the aqueous phase. Four model particle morphologies are selected for calculation.

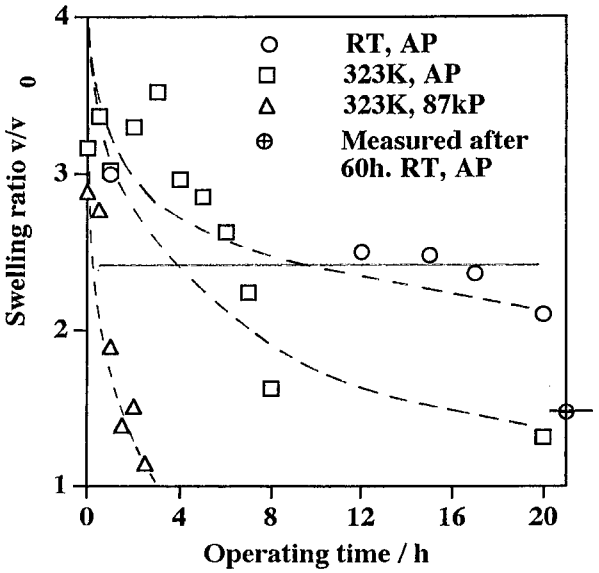

RT = room temperature, AP = atmospheric pressure, kP = 1000 Pa.

Figure 9 Swelling ratio during the stripping operation. Intensity of the stripping is changed.

with TEM. The TEM photographs of the stained particles corresponding to the stripping condition are shown in Figure 10 together with the OM photos. The core (PS)-shell (PMMA–styrene 4:14) morphology was obtained, except for the particles exposed to the most vigorous stripping (case A).

This simple investigation clearly indicated that the salami-like morphologies as shown in Figure 8 were kinetically controlled. Once the frozen state was relieved, they settled to the thermodynamically favored state, the core-shell morphology.

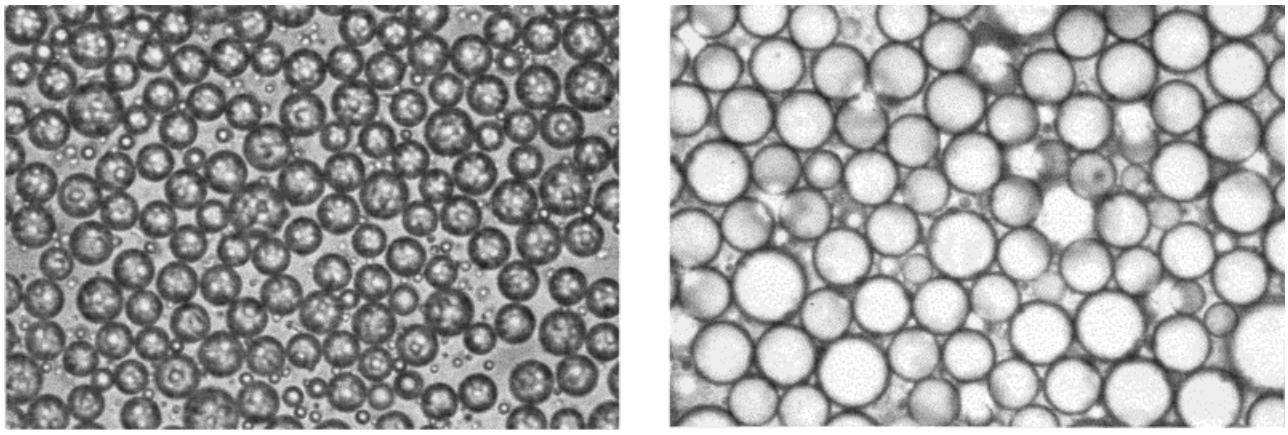

Figure 8 Optical photographs of P(MMA–co-styrene)/PS composite particles (run 5816) before and after the swelling with toluene. Smaller droplets in the left photo indicates the droplets of toluene.

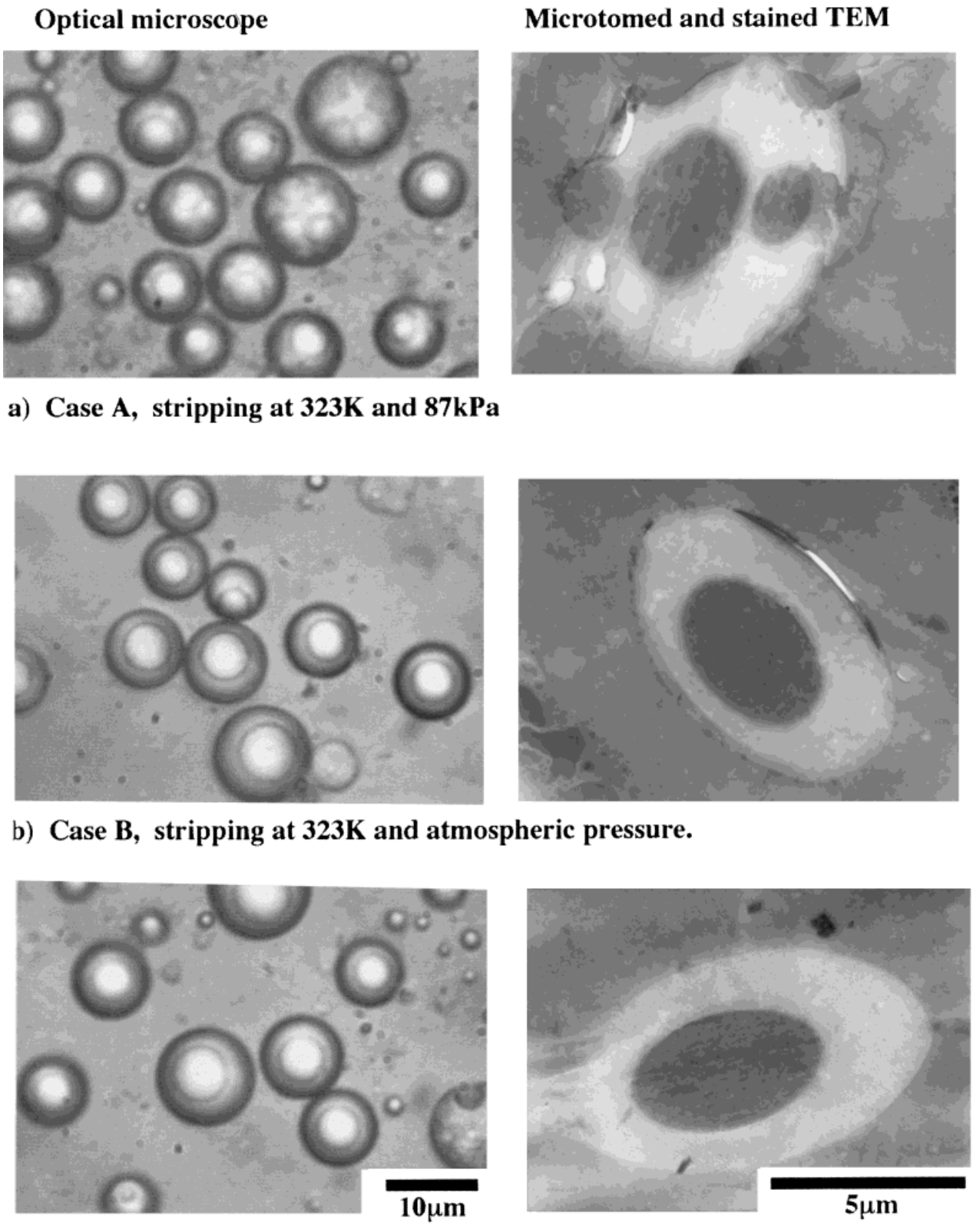

Figure 10 Settled morphologies after the stripping. Thermodynamically favored morphology is PS(core)/P(MMA–co-styrENE) (shell) as shown in cases B and C.

Morphology of Copolymer Particles Formed From a Monomer Pair With Widely Different Reactivity Ratios

In the previous section, the morphologies of composite polymer particles formed from two immiscible (co)polymers were discussed. One of the polymer was dissolved in the other monomer, and the morphology developed, whereas the latter was polymerized.

It is well known that in batch copolymerization, a noticeable composition drift in copolymer is observed whenever the reactivity ratios between two monomers are widely different. If we could find a particular monomer pair, a delicate morphology created from the composition drift of copolymers may be detected owing to the advantage of larger polymer particles. Besides having widely different reactivity ratios, the monomers are desirably both hydrophobic, and one of the homopolymer is stainable with RuO_4, whereas the other is not. This is not easy to fulfill. For example, styrene (r = 0.4) and acrylonitrile (r = 0.04) satisfy the condition for reactivity ratios, however the latter is quite hydrophilic and both domains are stained with RuO_4. Also, the monomer pair must form a random copolymer ($r_1r_2 < 1$). We searched for possible styrene (stainable)-acrylate (not stainable) pair and finally settled in styrene (r_S = 0.70) and cyclohexyl acrylate (CHA, r_{CHA} = 0.17).[30] The instantaneous composition of CHA in copolymer is plotted against the monomer conversion in Figure 11. It can be easily understood that, compared with styrene (r_S = *0.54) − MMA (*r_{MMA} = 0.46) pair, the polymers formed in the last stage of copolymerization is overwhelmingly rich in CHA, even though the initial monomer composition is a moderate 50:50.

The formulation for CHA-styrene emulsion is listed in Table V. Low and high initiator concentration runs were scheduled in order to investigate the effect of polymer chain length to the resulting particle morphology. BPO was dissolved in the mixture of monomers and then permeated through the membrane. The results of emulsification and polymerization are shown in Table VI. Normally, it is an easy procedure to separate the 25 wt % water contained in BPO from the oil phase. However, in this oil phase, the water was not separated completely, and some remained in the oil phase when it was permeated through the SPG membrane. Inevitably, the membrane pores were wet with the oil phase, resulting in scattered droplet sizes and CV as shown in Table VI. The

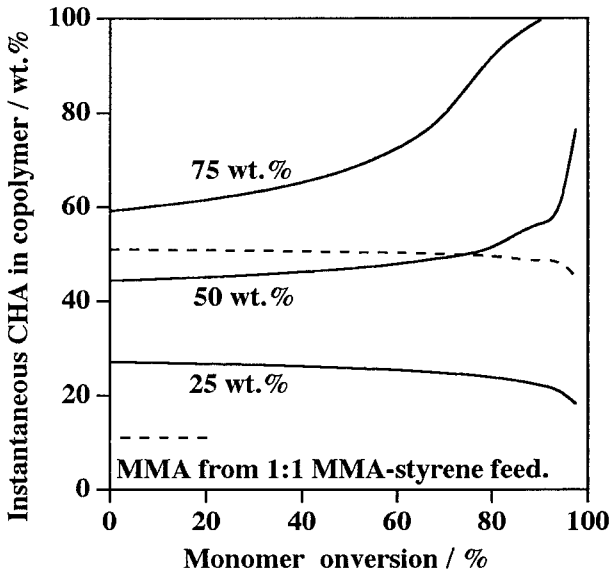

Figure 11 Instantaneous copolymer composition (CHA) against overall monomer conversion. Calculated using terminal model.

normal droplet size with a 1.4-μm membrane pore is 8–10 μm.

However, the resultant latex particles maintained spherical shape, and no significant coagulation occurred during the polymerization except run 5865, in which quite a few polymer particles were coagulated probably due to the lower T_g and lower molecular weight. All the latices were quenched with ice water immediately after the polymerization to save the particle morphology.

As the observation of latices by optical microscope revealed no particular difference in particle morphologies, TEM observation of microtomed specimen stained with RuO_4 was carried out. The photographs are shown in Figure 12. The effects of molecular weight (chain length) and glass transition temperature to the particle morphology can be detected in the two sets of experiments with increasing feed composition of CHA. The CHA-rich domains (white spots) are scattered in the dark styrene-rich matrices as shown in Figure 12(c)–(f). In the comparison between run 5860 (c) and 5864 (d) (CHA/styrene = 10/10), the domain size seemed to be smaller, and the number of domains increased as the molecular weight of copolymers decreased. By contrast, the comparison between run 5862 [Fig. 12(e)] and 5865 [Fig. 12(f)] (CHA/styrene = 15/5) showed the larger domain sizes in the latter, supporting the general theory that the shorter chains are more mobile than the longer chains, and are capable to form larger size

Table V Formulation for Cyclohexyl Acrylate (CHA)/Styrene Emulsion (in grams)

	Run No.					
Ingredients	5861	5860	5862	5863	5864	5865
CHA	5.0	10.0	15.0	5.0	10.0	15.0
Styrene	15.0	10.0	5.0	15.0	10.0	5.0
BPO	0.2	0.2	0.2	1.0	1.0	1.0
Water	180	180	180	180	180	180
PVA	1.0	1.0	1.0	1.0	1.0	1.0
SLS	0.027	0.027	0.027	0.027	0.027	0.027
Na_2SO_4	0.033	0.033	0.033	0.033	0.033	0.033
Hydroquinone	0.013	0.013	0.013	0.013	0.013	0.013

CHA, cyclohexyl acrylate; BPO, benzoyl peroxide; PVA, polyvinyl alcohol; SLS, sodium lauryl sulfate.

domains. It is clear from Figure 11 that copolymers having high CHA composition only formed toward the end of polymerization. The spheres of run 5860 contained less CHA-rich domains because of the lower final monomer conversion (61.5%). Also, from Table VI, the observed T_g for run 5860 (337 K) and 5864 (338 K) are pretty close to the reaction temperature (343 K). It is speculated that the high viscosity of the matrix polymer prevented the CHA-rich domains from growing further to form large domains compared with run 5865, which revealed much lower T_g (321 K).

CONCLUSIONS

Advantages of the SPG emulsification and the subsequent suspension polymerization were demonstrated for investigations of polymer particle morphology, control of which plays a vital role for commercial latex synthesis. Uniform 10-μm polymer particles provided ideal observation sites for varieties of particle morphology analysis, which have been limited to submicron scales. In this article, thermodynamically and kinetically controlled morphologies were investigated by selecting various controlling factors such as the differ-

Table VI Experimental Results of P(CHA-Co-styrene) Copolymer Spheres

	Run No.					
	5861	5860	5862	5863	5864	5865
d_e (μm)	21.3	9.25	13.4	24.8	16.7	21.7
CV (%)	14.7	11.6	12.1	22.3	15.8	23.6
d_p (μm)	17.6	7.76	12.5	20.2	14.9	17.6
CV (%)	21.6	13.8	17.4	22.6	20.7	22.3
Monomer conversion (%)	52.4	61.5	84.2	84.6	84.8	28.1[a]
$T_{g,\mathrm{calc}}$ (K)[b]	348	328	309	348	328	309
$T_{g,\mathrm{obs}}$ (K)	345	337	313	351	338	321
Mol wt						
$M_n(\times 10^{-4})$	6.18	6.07	5.81	1.76	2.40	1.26
$M_w(\times 10^{-4})$	12.6	13.8	15.0	4.28	5.61	8.74
M_w/M_n	2.04	2.27	2.58	2.43	2.34	6.91

CV, coefficient of variations.
[a] The latex was unstable, and most polymer particles were coagulated.
[b] Calculated from the Fox equation.

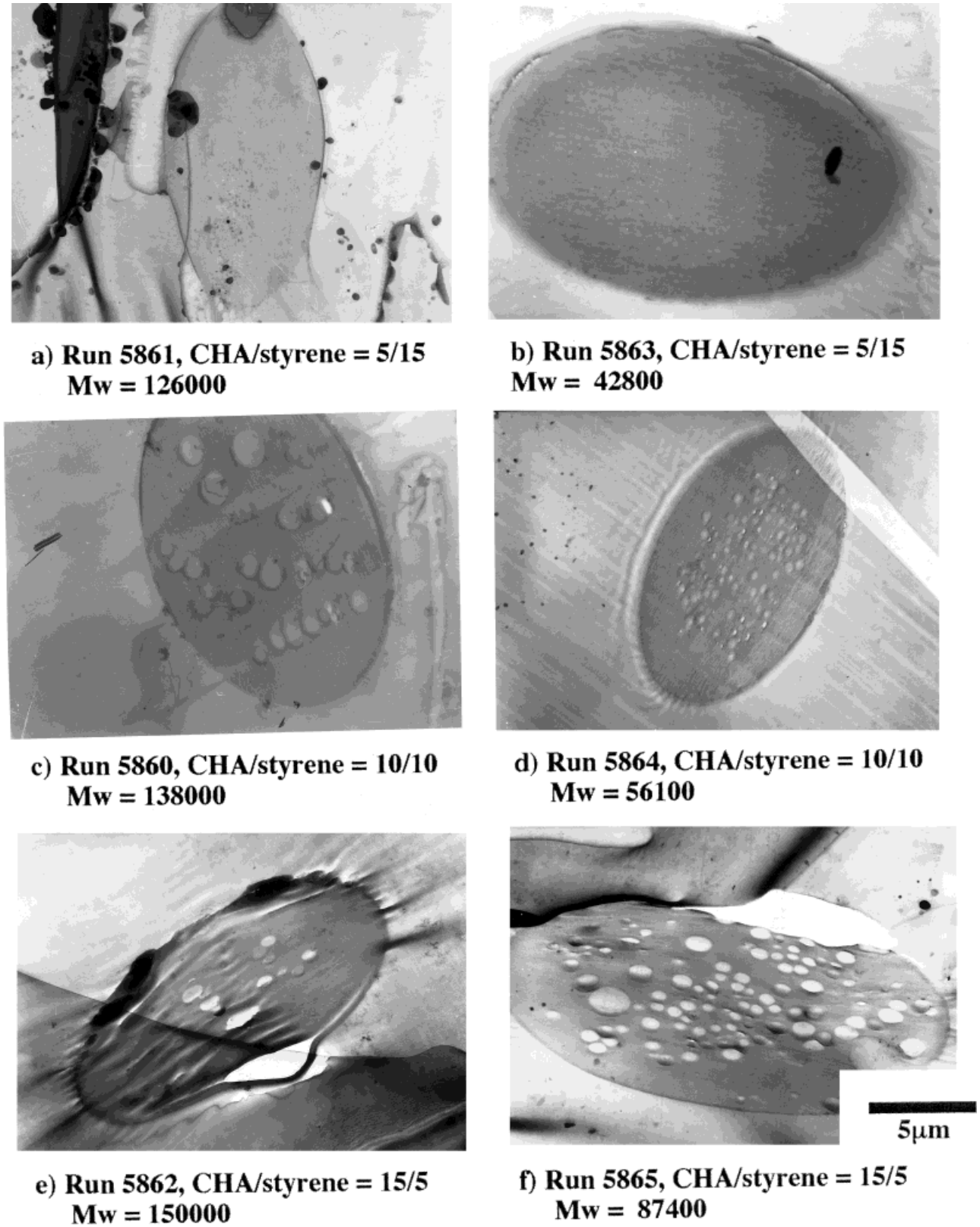

Figure 12 Microtomed and RuO_4-stained TEM photographs showing particle morphologies developed because of the composition drift. Effect of molecular weight can be detected by comparing (c) and (d), and (e) and (f).

Table A.I. Surface and Interfacial Tensions Used in This Study

Phase or Interphase	Tension (mN/m)
Surface tension	
Aqueous phase[a]	48.23
Oil phase A[b]	29.78
Oil phase B[c]	29.94
Oil phase C[d]	30.02
PMMA	41.40[e]
Polystyrene	40.70[e]
Interfacial tension	
Oil phase A/aqueous phase	3.631
Oil phase B/aqueous phase	3.940
Oil phase C/aqueous phase	3.526
PMMA/aqueous phase	19.98
P(MMA-co-styrene)/aqueous phase	29.55
Polystyrene/aqueous phase	31.00
Oil phase A/PMMA	11.95
Oil phase B/PMMA	11.68
Oil phase C/PMMA	11.57
Oil phase A/P(MMA-co-styrene)	12.39
Oil phase B/P(MMA-co-styrene)	11.23
Oil phase C/P(MMA-co-styrene)	11.23
Oil phase A/polystyrene	11.7
Oil phase B/polystyrene	10.92
Oil phase C/polystyrene	10.89

PMMA, polymethyl methacrylate; MMA, methyl methacrylate; PVA, polyvinyl alcohol. SLS, sodium lauryl sulfate.
[a] Water, 225 g; PVA, 1.5 g; SLS, 0.045 g; sodium sulfate, 0.03 g.
[b] Benzene, 19.5 g; hexadecane, 4.0 g; hexanol, 7.5 g.
[c] Benzene, 19.5 g; hexadecane, 4.0 g; hexanol, 15.0 g.
[d] Benzene, 19.5 g; hexadecane, 4.0 g; hexanol, 22.5 g.
[e] From Wu.[31]

ent mobilities between the components, compatibilities between the polymers, hydrophilicities, and reactivity ratios between the monomers.

MMA, MMA-styrene 50:50, and styrene were emulsified with a mixture of solvents composed of hexanol, benzene, and hexadecane. Hydrophilicity of the mixed solvent was adjusted by changing the amount of HA, whereas the amounts of benzene and HD were fixed. Resulting particle morphologies after the polymerization of hydrophilic MMA were the typical hemisphere, sandwich, and core (PMMA)-shell(solvent) depending on the increasing hydrophilicity of the mixed solvent. With increasing composition of hydrophobic styrene, the morphologies shifted from hemisphere core/solvent shell to raspberry core/solvent shell. Interestingly, these morphologies were eventually converted to polymer core/solvent shell except for the hemisphere composed of PMMA and the least hydrophilic mixed solvent.

When polystyrene (less mobile than the above mixed solvent) was dissolved in the mixture of MMA and styrene, and the droplets were polymerized, the resulting morphologies changed from salami to core-shell as the fraction of hydrophilic MMA in the monomer mixture became higher, demonstrating nonequilibrium, kinetically frozen morphologies. These salami particles were converted to core-shell after swelling by toluene and the gradual removal of the solvent under the mild stripping conditions.

Finally, when styrene and cyclohexyl acrylate—a pair having distant values of reactivity ratio, 0.70 and 0.17, respectively—were copolymerized, salami morphologies with tiny domains of CHA-rich phase dispersed in the matrix polymers were observed. Copolymer overwhelmingly rich in CHA was predicted to form in the final stage of polymerization from the calculations according to the terminal model, and the mobility of the copolymers was, at least to some extent, restricted by the increasing viscosity in the droplets, producing the salami-like morphology.

REFERENCES

1. Vitali R.; Montani E. Polymer 1980, 21, 1220.
2. Trent, J. S.; Scheinbeim, J. L.; Couchman, P. R. Macromolecules 1983, 16, 589.
3. Vanderhoff, J.W. In Future Directions in Polymer Colloids; El-Aasser, M. S., Fitch, R. M., Eds.; NATO ASI Series; 1987, E138, p 23.
4. Shen, S.; El-Aasser, M. S.; Dimonie, V. L.; Vanderhoff, J. W.; Sudol, E.D. J Polym Sci Polym Chem Ed 1991, 29, 857.
5. Ottewill, R. H. In Scientific Methods for the Study of Polymer Colloids and Their Applications; Candau, F., Ottewill, R. H., Eds.; NATO ASI Series; 1990, C303, p 349.
6. Winnik, M. A.; Croucher, M. D. In Future Directions in Polymer Colloids; El-Aasser; M. S., Fitch, R. M., Eds.; NATO ASI Series; 1987, E138, p 277; Winnik, M. A.; Peckan, O.; Croucher, M. D. In Scientific Methods for the Study of Polymer Colloids and Their Applications; Candau, F., Ottewill, R. H. Eds.; NATO ASI Series; 1990, C303, p 225.
7. Ottewill, R. H. In Future Directions in Polymer Colloids; El-Aasser, M. S., Fitch, R. M., Eds.; NATO ASI Series; 1987, E138, p 253.
8. Landfester, K.; Boeffel, C.; Lambla, M.; Spiess, H. W. Macromol Symp 1995, 92, 109; Landfester, K.; Spiess, H. W. In Polymeric Dispersions; Principles and Applications; Asua, J. M., Ed.; NATO ASI Series; 1997, E335, p 203.

9. Maron, S. H.; Elder, M. E.; Ulevitch, I. N. J Colloid Sci 1954, 9, 89.
10. Pijpers, A. P. In Scientific Methods for the Study of Polymer Colloids and Their Applications; Candau, F., Ottewill, R. H., Eds.; NATO ASI Series; 1990, C303, p 291.
11. Fitch, R. M. Polymer Colloids; Academic Press: San Diego, CA, 1997.
12. Dimonie, V. L.; Daniels, E. S.; Shaffer, O. L.; El-Aasser, M. S. In Emulsion Polymerization and Emulsion Polymers; Lovell, P. A., El-Aasser, M. S., Eds.; John Wiley & Sons: New York, 1997.
13. Sundberg, D. C. J Appl Polym Sci 1990, 41, 1425; Winzor, C. L.; Sundberg, D. C. Polymer 1992, 33, 3797, 4269; Sundberg, D. C.; Durant, I. G. In Polymeric Dispersions; Principles and Applications; Asua, J. M., Ed.; NATO ASI Series; 1997, E335, p 177.
14. Chen, Y. C.; Dimonie, V. L.; El-Aasser, M. S. J Appl Polym Sci 1991, 41, 1049; Macromolecules 1991, 24, 3779; J Appl Polym Sci 1992, 45, 487.
15. Sundberg, E. J.; Sundberg, D. C. J Appl Polym Sci 1993, 47, 1277.
16. Gonzalez-Ortiz, L. J.; Asua, J. M. Macromolecules 1005, 28, 3135; Macromolecules 1996, 29, 383, 4520.
17. Omi, S.; Katami, K.; Taguchi, T.; Kaneko, K.; Iso, M. Macromol Symp 1995, 92, 309.
18. Omi, S. Colloid Surf A 1996, 97, 109.
19. Omi, S.; Nagai, M.; Ma, G.-H. In Second World Congress on Emulsion; Bordeau, France, 1997, vol 4, p 99.
20. Omi, S.; Nagai, M.; Ma, G.-H. Macromol Symp 2000, 151, 319.
21. Ma, G.-H.; Nagai, M.; Omi, S. Colloid Surf A 1999, 153, 383.
22. Ma, G.-H.; Nagai, M.; Omi, S. J Colloid Interface Sci 1999, 214, 264.
23. Ma, G.-H.; Nagai, M.; Omi, S. J. Colloid Interface Sci 1999, 219, 110.
24. Omi, S.; Katami, K.; Yamamoto, Y.; Iso, M. J Appl Polym Sci 1994, 51, 1.
25. Omi, S.; Katami, K.; Taguchi, T.; Kaneko, K.; Iso, M. J Appl Polym Sci 1995, 57, 1013.
26. Omi, S.; Taguchi, T.; Nagai, M.; Ma, G.-H. J Appl Polym Sci 1997, 63, 913.
27. Brandrup, J.; Immergut, E. H. Polymer Handbook; 3rd Ed.; 1989, vol VII, p 519.
28. Yuyama, H.; Nagai, M.; Ma, G.-H.; Omi, S. J Appl Polym Sci 2000, 78, 1025.
29. Fitch, R. M., private communication, 1994, June 2.
30. Brandrup, J.; Immergut, E. H. Polymer Handbook; 3rd Ed., 1989, vol II, p 153.
31. Wu, S. Polymer Blend. Vol 1; Academic Press: San Diego, CA, 1978.